


Original Article

Fenton reaction-induced renal carcinogenesis in *Mutyh*-deficient mice exhibits less chromosomal aberrations than the rat model

Guang Hua Li,¹ Shinya Akatsuka,¹ Shan Hwu Chew,¹ Li Jiang,¹ Takahiro Nishiyama,² Akihiko Sakamoto,^{2*} Takashi Takahashi,³ Mitsuru Futakuchi,⁴ Hiromu Suzuki,⁵ Kunihiko Sakumi,⁶ Yusaku Nakabeppu⁶ and Shinya Toyokuni ^{1,7}

¹Department of Pathology and Biological Responses, Nagoya University Graduate School of Medicine, Nagoya 466-8550, Japan, ²Department of Hematology and Oncology, Nagoya University Graduate School of Medicine, Nagoya 466-8550, Japan, ³Division of Molecular Carcinogenesis, Center for Neurological Diseases and Cancer, Nagoya University Graduate School of Medicine, Nagoya 466-8550, Japan, ⁴Department of Molecular Toxicology, Nagoya City University Graduate School of Medical Sciences, Nagoya 467-8601, Japan, ⁵Department of Molecular Biology, Sapporo Medical University School of Medicine, Sapporo 060-8556, Japan, ⁶Division of Neurofunctional Genomics, Department of Immunobiology and Neuroscience, Medical Institute of Bioregulation, Kyushu University, Fukuoka 812-8582, Japan, and ⁷Sydney Medical School, The University of Sydney, NSW, Australia

Oxidative stress including iron excess has been associated with carcinogenesis. The level of 8-oxoguanine, a major oxidatively modified base in DNA, is maintained very low by three distinct enzymes, encoded by *OGG1*, *MUTYH* and *MTH1*. Germline biallelic inactivation of *MUTYH* represents a familial cancer syndrome called *MUTYH*-associated polyposis. Here, we used *Mutyh*-deficient mice to evaluate renal carcinogenesis induced by ferric nitrilotriacetate (Fe-NTA). Although the *C57BL/6* background is cancer-resistant, a repeated intraperitoneal administration of Fe-NTA induced a high incidence of renal cell carcinoma (RCC; 26.7%) in *Mutyh*-deficient mice in comparison to wild-type mice (7.1%). Fe-NTA treatment also induced renal malignant lymphoma, which did not occur without the Fe-NTA treatment in both the genotypes. Renal tumor-free survival after Fe-NTA treatment was marginally different ($P = 0.157$) between the two genotypes. Array-based comparative genome hybridization analyses revealed, in RCC, the loss of heterozygosity in chromosomes 4 and 12 without *p16^{INK4A}* inactivation; these results were confirmed by a methylation analysis and showed no significant difference between the genotypes. Lymphomas showed a preference for genomic amplifications. *Dlk1* inactivation by promoter

methylation may be involved in carcinogenesis in both tumors. Fe-NTA-induced murine RCCs revealed significantly less genomic aberrations than those in rats, demonstrating a marked species difference.

Key words: Fe-NTA, lymphoma, *Mutyh*-deficient mice, oxidative stress, renal cell carcinoma

Oxidative stress is caused by a variety of chemical, physical and biological agents and is associated with carcinogenesis.^{1,2} Iron excess may cause Fenton reaction-induced oxidative stress, and this is recognized as one of the causes of carcinogenesis^{3–5} based on human epidemiological data, such as in genetic hemochromatosis (hepatocellular carcinoma),⁶ endometriosis (ovarian cancer),^{7,8} viral hepatitis C (hepatocellular carcinoma)^{9,10} and asbestos-induced malignant mesothelioma.^{11,12}

We established an iron-induced renal carcinogenesis model in wild-type rats and mice using a repeated intraperitoneal administration of a redox-active iron chelate, ferric nitrilotriacetate (Fe-NTA).^{13–15} Renal cell carcinoma (RCC), induced by Fe-NTA in wild-type rats, reveals prominent chromosomal aberrations, and these patterns are extremely similar to those observed in human counterparts.¹⁶ In addition, this model provides a reproducible acute model of oxidative renal proximal tubular damage,^{17–19} where numerous oxidative stress markers are significantly increased in the kidney 3 h after a single administration of Fe-NTA, including 8-oxoguanine (8-oxoG)²⁰ and 4-hydroxy-2-nonenal.^{15,21,22}

The base 8-oxoG, a modified base in nucleotides after oxidative reactions, is most abundant as an oxidatively modified DNA base in the genome, but it may cause a G to

Correspondence: Shinya Toyokuni, MD, PhD, Department of Pathology and Biological Responses, Nagoya University Graduate School of Medicine, 65 Tsurumai-cho, Showa-ku, Nagoya, Aichi 466-8550, Japan. Email: toyokuni@med.nagoya-u.ac.jp

*Present address: Department of Mechanism of Aging, National Center for Geriatrics and Gerontology, Obu 474-8511, Japan.

Received 15 August 2017. Accepted for publication 20 September 2017.

© 2017 Japanese Society of Pathology and John Wiley & Sons Australia, Ltd

T transversion-type mutation when it is present at DNA replication; therefore, it represents a premutagenic lesion.²³ The base 8-oxoG is present in the nuclear genome of cells at a level of approximately 1 in 10⁶ guanines in non-pathologic conditions, which is equilibrated both by the increase in 8-oxoG by the persistent generation of reactive oxygen species (ROS) and by its decrease by repair via two distinct enzymes encoded by *OGG1* or *MUTYH* and sanitization of nucleotide pool by *MTH1*.²⁴ The germline biallelic inactivation of *MUTYH* represents a familial cancer syndrome called *MUTYH*-associated polyposis in humans.^{25,26}

We are aware, from our previous experiments, that the *C57BL/6* background is resistant to carcinogenesis,^{14,27} including that by Fe-NTA (unpublished data, H Ohara and S Toyokuni), whereas various strains of rats examined were all sensitive (~90% incidence in Wistar/Fischer-344/Brown-Norway strains).^{28,29} *Mutyh*-deficient mice of the *C57BL/6* background show a higher incidence of spontaneous or carcinogen-induced carcinogenesis in comparison to their wild-type counterparts.³⁰ Here, we used *Mutyh*-deficient mice to evaluate the difference in renal carcinogenesis induced by Fe-NTA between rats and mice. Unexpectedly, we found a marked species difference in the genomic alteration of Fe-NTA-induced RCC.

MATERIALS AND METHODS

Materials

Ferric nitrate enneahydrate and nitrilotriacetic acid (NTA) disodium salt were from Wako (Osaka, Japan) and were dissolved in deionized water to make 300 mM and 600 mM solutions, respectively. The Fe-NTA solution was prepared immediately before use by mixing these at a volume ratio of 1:2 (molar ratio 1:4) and adjusting the pH to 7.4 with sodium carbonate as described.²¹ The rabbit monoclonal antibody against Ki67 was from Abcam (ab16667; Cambridge, UK), and the mouse monoclonal antibody against 8-hydroxy-2'-deoxyguanosine (8-OHdG; also as 8-oxoG for modified base in DNA) was from Nikken Seil (Fukuroi, Japan). A rat monoclonal antibody (RA3-6B2) for immunohistochemistry, recognizing mouse B220 (CD45R) as a B-cell marker, was from BD Pharmingen (San Diego, CA, USA).³¹ A rabbit polyclonal antibody for immunohistochemistry, recognizing the CD3 ϵ chain as a T-cell marker, was from Abcam (ab5690). A rat monoclonal antibody (30-F11, PerCP) for FACS analyses, recognizing mouse CD45 as a pan-leukocyte marker, was from BioLegend (San Diego, CA, USA). A rat monoclonal antibody (eBio1D3, PE) for FACS analyses, recognizing mouse CD19 as a B-cell marker, was from eBioscience (San Diego, CA, USA). An Armenian

hamster monoclonal antibody (145-2C11, APC-eFluor) for FACS analyses, recognizing the mouse CD3 ϵ chain as a T-cell marker, was from eBioscience.

Genotyping the *Mutyh*^{+/-} mice and animal experiments

Mutyh^{+/-} mice with a *C57BL/6* background were generated as described previously.³⁰ All the mice used for the experiments were obtained by crossing heterologous *Mutyh*^{+/-} mice. The primer pairs used to detect the wild-type and mutant alleles were as follows: 5'-CCTGGTGCAAAGGCCTGA-3' (forward) and 5'-GCAGTAGACACAGCTGCAT-3' (reverse) primers for the wild-type allele, and 5'-CTACG CATCG GTAATGAAGG-3' as the forward *neo* primer and the same reverse primer for the mutated allele. All the animals were maintained in an air-conditioned specific pathogen-free room with a time-controlled lighting system. The Animal Experiment Committee of Nagoya University Graduate School of Medicine approved all the protocols. Only male mice were used for its higher sensitivity to Fe-NTA.¹⁹

Protocol for Fe-NTA-induced renal carcinogenesis in mice

There were four groups of 20 male mice at the start of the carcinogenesis study: *Mutyh*^{+/+} and Fe-NTA treatment; *Mutyh*^{-/-} and Fe-NTA treatment; *Mutyh*^{+/+} with no treatment; and *Mutyh*^{-/-} with no treatment. We used 8- to 9-week-old male mice that each weighed 22–24 g. Fe-NTA was injected intraperitoneally (ip) at a dose of 3 mg iron/kg five times a week for the first week, which was thereafter increased to 5 mg iron/kg five times a week during the next 11 weeks. The mice were euthanized when they appeared ill or showed >5% weight reduction in a week. Finally, at around 120 weeks, the final effective numbers of mice in each group were 14, 15, 16 and 19, respectively, accounting for the reduction of early accidental death. A complete autopsy was performed, and the tissue samples were either fixed with 10% PBS-buffered formalin for routine pathological examination, frozen at -80°C until use for other analyses, or were directly filtered through cell strainer for primary culture, followed by FACS analyses.

Fe-NTA-induced renal subacute toxicity protocol in mice

For the subacute experiments, 11 male *Mutyh*^{+/+} and 12 male *Mutyh*^{-/-} mice were used. The Fe-NTA treatment was as follows: 3, 0, 3, 3, 3, 5, 5 and 5 mg iron/kg ip administration was performed at approximately 10 am each day. The mice were euthanized 48 h after the final

administration of Fe-NTA. The kidneys were immediately dissected and fixed with 10% PBS-buffered formalin for routine pathological examination or immunohistochemistry.

Histological and immunohistochemical analyses

These analyses were performed as described³¹ except for the use of BOND MAX/III (Leica, Wetzlar, Germany). The quantitative analyses were performed both for the areas and the integrated density as described,³¹ except that ImageJ was used (<https://imagej.nih.gov/ij/>) as the software.

FACS analyses of malignant lymphoma cells

The obtained nodule of malignant lymphoma was filtered through a Falcon cell strainer (Ref#352350, 70 μ m; Corning; Corning, NY) into RPMI medium with 10% fetal bovine serum, which was cultured on a feeder layer of BLS4 as described.^{32–35} After 8–10 passages, the floating lymphoma cells were used for the FACS analyses as described.³⁶

Array-based CGH (aCGH) analysis

We used the DNeasy Blood and Tissue Kit (QIAGEN GmbH, Hilden, Germany) to extract the genomic DNA, and the Quant-iT dsDNA BR Assay Kit (Life Technologies, Carlsbad, CA) was used to quantify the DNA. aCGH was performed with a Mouse Genome CGH Microarray 4 \times 180K (4839A; Agilent Technologies, Santa Clara, CA, USA) according to the Agilent Oligonucleotide aCGH for Genomic DNA Analysis Protocol, version 7.1. Genomic DNA from a normal wild-type mouse kidney was labeled with Cy3 as the reference. Selected tumor samples, including 4 RCCs and eight lymphomas, were labeled with Cy5. The Agilent Genomic Workbench Standard Edition (version 5.0) was used to analyze the results.

Methylation analysis by bisulfite pyrosequencing

The analysis was carried out as described previously.³⁷ Genomic DNA (1 μ g) was modified with sodium bisulfite using the EpiTect Bisulfite Kit (Qiagen), and after which, target segments in the genome were amplified with specific PCR primer pairs (Table S1) with 5' end of reverse primer modified with biotin. Pyrosequencing was then performed using a PSQ96 system with a PyroGold reagent Kit (Qiagen). For the pyrosequencing, the biotinylated PCR product was purified, made single-stranded and used as a template in a pyrosequencing reaction run according to the manufacturer's instructions. We used multiple sequencing

primers for some of the PCR products to analyze different CpG sites (Table S1). The results of the bisulfite pyrosequencing were analyzed using Q-CpG software (Qiagen).

Mutational analysis of *Cdkn2a* gene

Genome DNA of four RCCs was subjected to PCR amplification for mutation analyses. All the four exons in *Cdkn2a* gene were amplified, using primers shown in Table S2. Direct DNA sequencing was performed, using Applied Biosystems 3100 Genetic Analyzer.

Comparison of the chromosomal alterations in Fe-NTA-induced RCC between mice and rats

To compare the extent of the chromosomal alterations in RCC between mice and rats, we calculated the percentage of chromosomal sites with a copy number aberration among all the sites in the whole genome as a quantitative measure. The copy number aberration frequency was calculated from the results of each aCGH analysis according to the following procedure: (i) compute a moving average of the signal log₂ ratios for the CGH microarray probes distributed within 500 kbp from each point at every 100 kb along the chromosomes; (ii) plot values of the moving averages of the signal log₂ ratios from the whole genome as a histogram, and determine the thresholds on both sides, beyond which, the copy number aberration can be called via a visual evaluation of the histogram for each aCGH result; and (iii) calculate the fraction of the chromosomal sites at which the copy number aberration was called according to the above defined thresholds.

We used the aCGH data from Fe-NTA-induced rat RCCs we previously published (GEO accession: GSE36101) to compare with the mouse data in the present study. Although the rat data includes the results from 13 primary tumors, the data from two primary tumors are omitted here because the background noise levels were too high. Figure S1 shows the histograms for the aCGH data used for this comparison analysis. The copy number aberration frequency is equivalent to a fraction of the genomic sites, which corresponds to red bars in the histogram for each aCGH result (Fig. S1).

STATISTICAL ANALYSIS

The Kaplan–Meier analysis and other statistical analyses were performed using GraphPad Prism software (GraphPad Software Inc., San Diego, CA). *P*-values for the Kaplan–Meier analysis were calculated by the log-rank test. Other analyses were assessed by the unpaired *t*-test, modified for unequal variances when necessary, and a Fisher's exact test. *P* < 0.05 was considered statistically significant.

RESULTS

Subacute study on Fe-NTA-induced renal carcinogenesis exhibits more oxidative stress with increased proliferation in the proximal tubular cells of *Mutyh*^{-/-} mice

We performed a subacute analysis on both the genotypes to evaluate the difference at an early stage of Fe-NTA-induced renal carcinogenesis. We observed renal proximal tubular degeneration in the kidney of the Fe-NTA-treated mice, which was not observed in the control mice (Fig. 1a–d). A histopathological analysis, after the Fe-NTA treatment, revealed simultaneous regenerative changes, such as nuclear enlargement in the renal proximal tubular cells with lymphocyte infiltration, which was more prominent in the *Mutyh*^{-/-} mice in comparison to the *Mutyh*^{+/+} mice (Fig. 1b, d). Immunostaining with 8-OHdG (also as 8-oxoG), after the Fe-NTA treatment, showed stronger nuclear staining in the renal proximal tubular cells of the *Mutyh*^{-/-} mice compared to those of the *Mutyh*^{+/+} mice (Fig. 1e–h,m) and a higher Ki-67 index in the *Mutyh*^{-/-} mice (Fig. 1i–l,n).

Tumor-free survival after Fe-NTA-induced renal carcinogenesis was marginally reduced in the *Mutyh*^{-/-} mice

Figure 2a–d displays the Kaplan–Meier curve of the renal tumor-free survival in each group. There was only a marginal difference in the survival of both the genotypes in the Fe-NTA-treated groups, whereas there was no difference in both the genotypes in the control groups. The difference in renal tumor-free survival between the Fe-NTA treatment and the untreated control was greater in the *Mutyh*^{-/-} mice. We observed four cases of RCC in the *Mutyh*^{-/-} mice in comparison to only one case in the *Mutyh*^{+/+} mice (Table 1 and Fig. 2e–h). Notably, we also observed non-Hodgkin's malignant lymphoma developing in the kidney in one case of the *Mutyh*^{-/-} mice and two cases in the *Mutyh*^{+/+} mice (Table 1 and Fig. 3a). All the tumors are numbered and described more in detail in Table S3.

aCGH analysis of RCC

A histopathological analysis of the RCC revealed proliferation of atypical tubular cells in papillary, glandular or solid patterns. The carcinoma cells were basophilic, and clear cells were not observed (Fig. 2g,h). We then performed an aCGH analysis of these RCC samples. One was of a microscopic size, which was thus excluded from the analysis. In the four samples, we observed wide areas of

common hemizygous loss in chromosome 4 (including the *p16/p15* tumor suppressor loci) and chromosome 12 (GEO accession: GSE99535). Chromosomes 4 and 12 in the mice corresponded to chromosomes 5 and 6 in the rats, respectively.³⁸ Hemizygous losses of those chromosomes were also observed at a high frequency in our previous study, using a Fe-NTA-induced rat RCC model.¹⁶ There was no obvious difference in the pattern of chromosomal copy number changes between the *Mutyh*^{-/-} and the *Mutyh*^{+/+} mice (Fig. 2i).

aCGH analysis of malignant lymphoma

Since, for the first time, we observed lymphoma in the kidneys of the Fe-NTA-treated mice (Fig. 3a), we performed an immunohistochemical staining and FACS analysis for confirmation. We observed destruction of the normal lymph node structure and replacement by a diffuse proliferation of atypical lymphocytes (Fig. 3b,c), revealing CD3 (T-cell marker) negativity and CD45R (B220; B-cell marker) positivity (Fig. 3d,e). We cultured the lymphoma cells with feeder cells, and performed a FACS analysis. We found that these cells were positive for CD45 and CD19 but negative for CD3, confirming that the lymphomas were B-cell type (Fig. 3f,g). We also performed an aCGH analysis on the lymphomas (GEO accession: GSE99535). However, in contrast to RCC, we did not detect hemizygous losses of chromosomes 4 and 12 in the lymphomas, but we detected more amplifications and less deletions at other chromosomal loci. We did not see a clear difference in the chromosomal alterations between the two genotypes (Fig. 3h,i).

Dlk1 loci are methylated in the RCC

We conducted methylation analyses of the promoter regions of 13 selected tumor suppressor genes, which are reported as methylated in human RCC or lymphoma. The results showed that more tumor suppressor genes were methylated in the promoter regions in the lymphomas compared to RCCs (Table 2). For RCC, methylation was observed only at the *Dlk1* locus on chromosome 12, which commonly exhibited a hemizygous loss (Fig. 2i). These methylations were not detected in any of the normal renal samples that were also analyzed as the reference.

No mutations in the *Cdkn2a* alleles of RCC

Direct sequencing analysis revealed no base-pair substitutions, insertions or deletions within the coding sequences in the *Cdkn2a* alleles in the 4 RCCs, implying that the RCCs can express *p16*^{INK4A} and *p19*^{ARF} proteins with the original amino acid sequences.

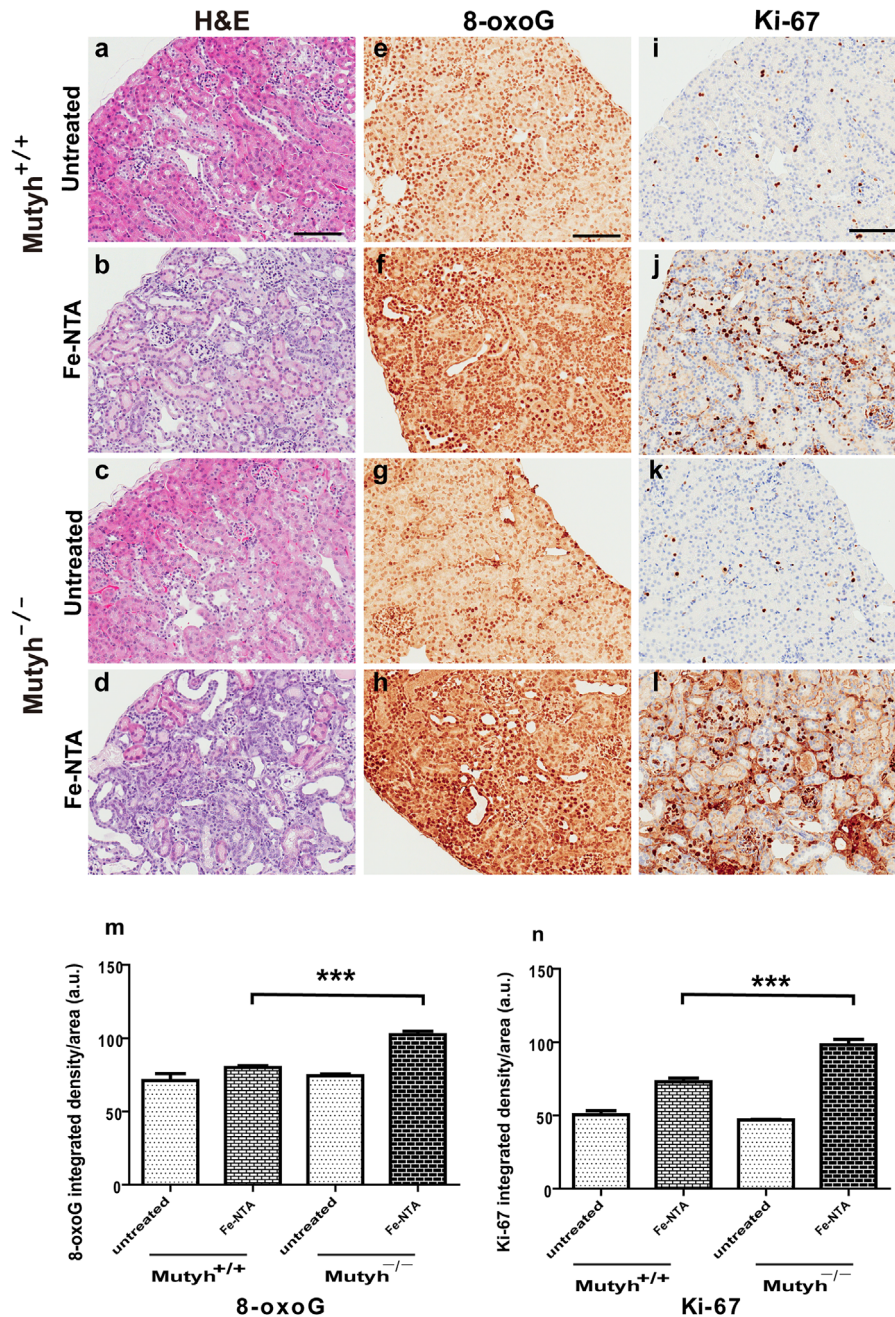


Figure 1 More oxidative stress in the kidney after a repeated intraperitoneal administration of Fe-NTA in *Mutyh*^{-/-} mice than wild-type mice in a subacute study. (a–d) Histology with immunohistochemical analysis of (e–h) 8-oxoG (8-OHdG) and (i–l) Ki-67. Fe-NTA treatment confers degenerative and regenerative renal proximal tubular cells simultaneously with increased nuclear staining of 8-oxoG and Ki-67, which is aggravated in *Mutyh*^{-/-} mice (bar = 100 μ m). Quantitation of the immunostained areas for (m) 8-oxoG and (n) Ki-67 (means \pm SEM). Refer to the text for details. *** $P < 0.001$. a.u., arbitrary unit.

Different predisposition to chromosomal alterations during renal carcinogenesis between mice and rats

We evaluated the predisposition of murine RCC to chromosomal changes. Essentially, we compared the present murine data with previously obtained rat RCC data (GEO accession: GSE36101), which were based on the copy

number aberration frequency calculated from the distributions of the signal log₂ ratios in each aCGH result. Overall, the copy number aberrations were less frequent in murine RCCs than in rat RCCs (Table 3 and Fig. S2). The total frequency of copy number aberration was significantly lower among murine RCCs than among rat RCCs (21.95% vs. 30.35%; $P < 0.001$, Fisher's exact test). In addition, the ratio

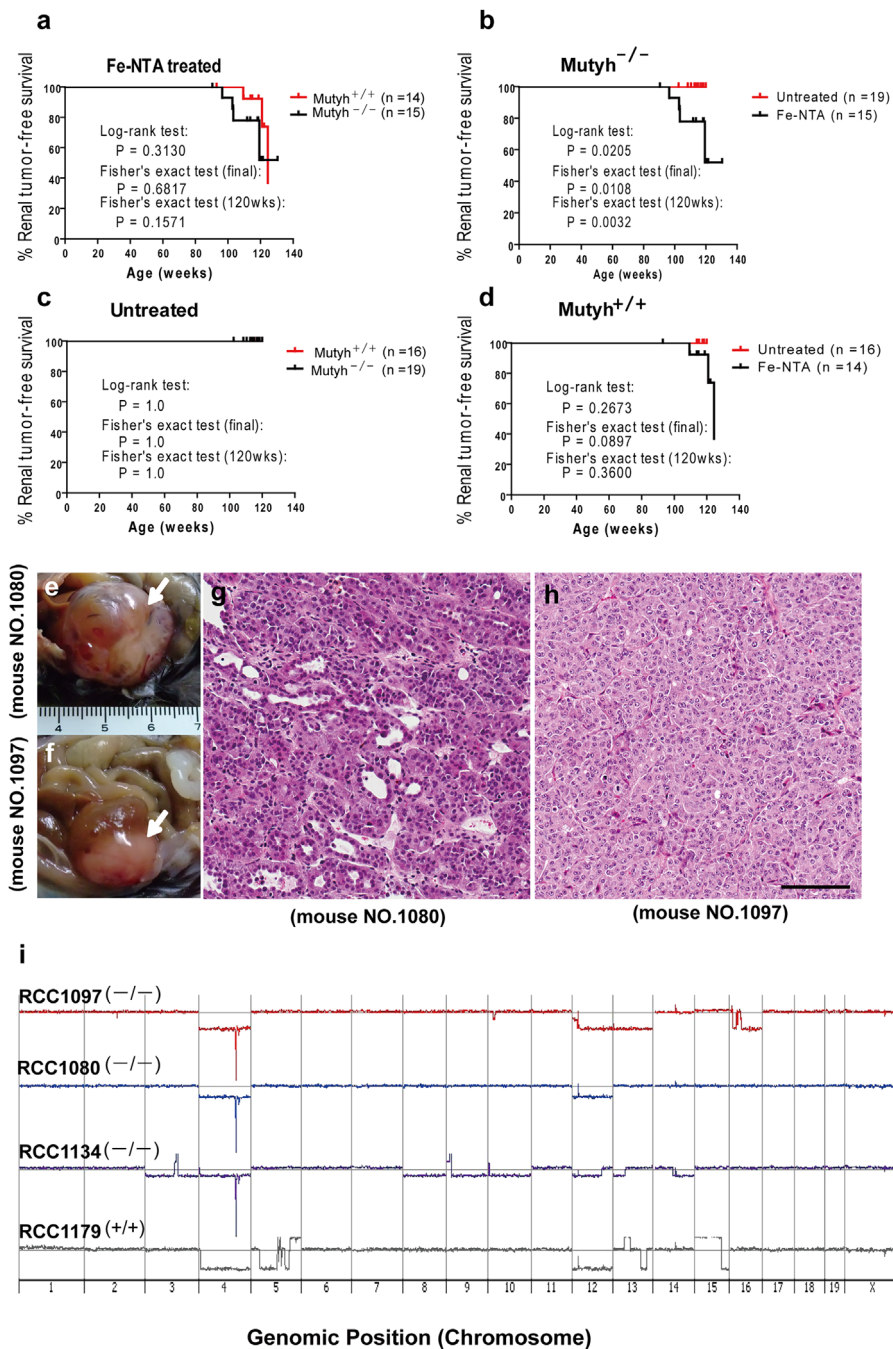


Figure 2 Marginal shortening of renal tumor-free survival during Fe-NTA-induced renal carcinogenesis in *Mutyh*^{-/-} mice with milder genetic alterations in RCCs by aCGH in both the genotypes than in rats. (a–d) Kaplan–Meier renal tumor-free survival curves. The tumors formed in the kidneys were counted here. Upper left, comparison among the Fe-NTA-treated mice (*Mutyh*^{-/-} vs wild-type); lower left, comparison among the untreated mice (*Mutyh*^{-/-} vs wild-type); upper right, comparison among the *Mutyh*^{-/-} mice (Fe-NTA treatment vs untreated); lower right, comparison among the wild-type mice (Fe-NTA treatment vs untreated). Fisher's exact tests were used to compare the renal tumor incidences between the two groups at 120 weeks. (e–h) Fe-NTA-induced RCC in mice with hematoxylin & eosin staining; arrows, indicating macroscopic view of RCC; atypical tubular cells are proliferating with a tubular or solid structure (bar = 100 μ m). (i) aCGH analysis of four murine RCC. The number below corresponds to each chromosome. A hemiallelic loss in chromosomes 4 and 12 was in common. A homozygous deletion in chromosome 4 of the *Mutyh*^{-/-} mice was induced during the gene knockout process and not the homozygous deletion of *p16* tumor suppressor gene. Rare gain/amplification and milder chromosomal aberrations in comparison to rat Fe-NTA-induced RCC. Refer to the text for details.

Table 1 Summary of tumor incidence

Organ/Genotype	Fe-NTA treatment		Untreated control	
	<i>Mutyh</i> (+/+)	<i>Mutyh</i> (-/-)	<i>Mutyh</i> (+/+)	<i>Mutyh</i> (-/-)
Kidney				
Renal cell carcinoma	1	4	0	0
Malignant lymphoma	2	1	0	0
Liver				
Hepatocellular carcinoma	0	0	1	0
Malignant lymphoma	1	1	0	1
Intestine				
Adenocarcinoma	0	0	1	1
Malignant lymphoma	2	3	0	2
Other organs				
Malignant lymphoma	1	1	2	2
Total number of tumors	7 in 4 mice (28.6%)	10 in 7 mice (46.7%)	4 in 4 mice (25.0%)	6 in 5 mice (26.3%)
Number of valid mice	14	15	16	19

Fe-NTA, ferric nitrilotriacetate. Refer to Table S3 and text for details.

of amplification to deletion in total was significantly lower among murine RCCs than among rat RCCs ($P < 0.001$, Fisher's exact test).

DISCUSSION

We obtained a higher incidence of Fe-NTA-induced RCC in the *Mutyh*-deficient mice in comparison to the wild-type counterparts in a carcinogenesis study of >2 years. This confirms a role of *MUTYH* in preventing oxidative stress-induced carcinogenesis,³⁰ despite the relatively small study. The renal tumor-free survival results were statistically marginal ($P = 0.1571$), which was presumably due to the size of each group and might be improved in a larger study in the future. The data in the subacute phase was consistent with the final carcinogenesis results in that 8-oxoG and the mitotic index by Ki67 were significantly higher in the *Mutyh*-deficient mice. The histology of RCC was similar to those in rats²⁸ or *A/J* mice,¹⁴ as we previously reported, and consisted of adenocarcinoma originating from renal tubular cells.

We also performed aCGH analyses on Fe-NTA-induced RCC, for the first time, in mice. However, because one of the RCC cases was cystic and too small (<1 mm), we analyzed only four samples. We noted a spiky homozygously deleted region in chromosome 4 in all the *Mutyh*-deficient mice analyzed (Figs. 2i,3i), which corresponds to around the 2 Mb region, approximately 3 Mb away from *Mutyh* locus toward the centromere (Fig. S3). The region is actually located within the residual block from the genome of CCE cell line, the embryonic stem cell used for the homologous recombination (Nakabeppu, Y. and Sakumi, K., unpublished data). There was no major distinction in the aCGH results of RCC between the two genotypes, and

basically, deletions were observed with a common region of hemiallelic loss in chromosomes 4 and 12 but with no common amplifications. Surprisingly, we found no homozygous deletion of $p16^{INK4A}/p15^{INK4B}$, which we previously hypothesized to be specific for iron-induced carcinogenesis, based on the data of rats and humans.^{5,16,39} Furthermore, the remaining allele of $p16^{INK4A}/p19^{ARF}$ was not inactivated in the RCCs with additional epigenetic and mutation analyses. In Fe-NTA-induced RCCs in rats, we observed numerous genomic locations of amplifications, and among which, a *c-Met* amplification was the most common.¹⁶ These results, using the same model in different species, suggest that murine carcinogenesis is different from those in rats and is much farther from those in humans.

In addition, we compared the frequency of the chromosomal aberrations in Fe-NTA-induced RCC between mice and rats. The chromosomal aberrations in murine RCC were significantly less than those in rat RCC. This may suggest that mice obtain cancer in fewer steps than rats. In this sense, the rat model may be more similar to human counterparts that occur sporadically. The mice model appears to be more similar to those of familial cancer syndromes or childhood cancers. Although the precise interpretation is difficult at the present time, possible hypotheses are as follows. It is easier for murine cells to put the proliferation-switch on, whereas proliferation is more rigorously regulated in rats; namely, in two-thirds of rat RCC cases induced by Fe-NTA, $p16^{INK4A}/p15^{INK4B}$ is inactivated either by a homozygous deletion or a heterozygous deletion/methylation,^{16,29} which indicates the loss of both brakes for the cell cycle and apoptotic pathways through TP53. We are aware that murine RCC is at a lower-grade malignancy in that we observed neither metastasis nor peritoneal invasion, whereas pulmonary metastases are quite common (~50%) in rat RCC.²⁸ Another possibility is that physical

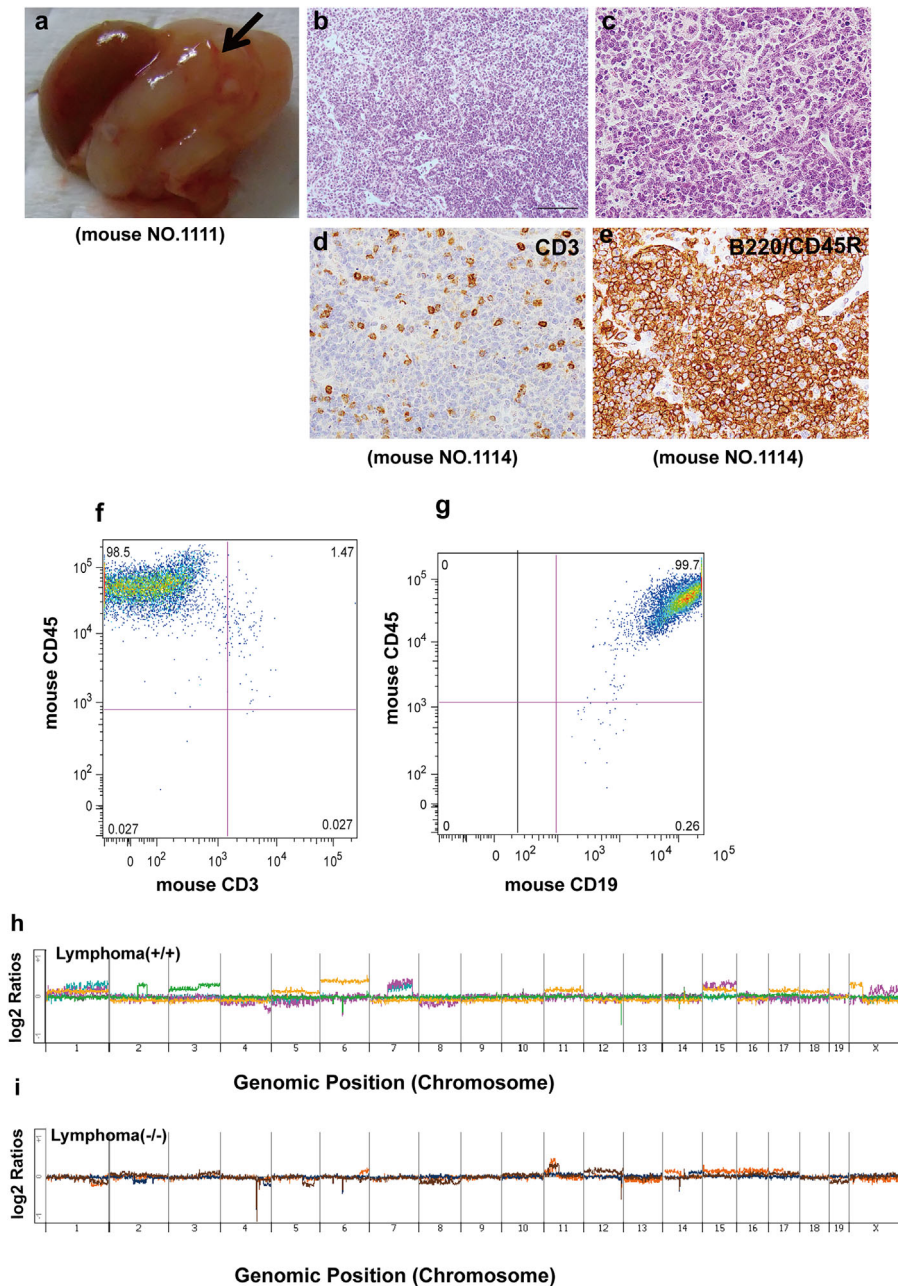


Figure 3 Malignant lymphomas in the kidney of Fe-NTA-treated mice of both the genotypes are B-cell type and reveal various chromosomal aberrations. (**a–e**) Macroscopic view of renal malignant lymphoma (**a**, arrow) after a Fe-NTA renal carcinogenesis protocol with histology after hematoxylin & eosin staining and immunohistochemistry for CD3 and B220/CD45R, with the diagnosis of non-Hodgkin B-cell lymphoma (bar = 100 μ m in (**b**) and 25 μ m in (**c–e**)). (**f** and **g**) FACS analysis of renal malignant lymphoma NO. 1114 confirmed the immunohistochemical data. (**h**) aCGH analysis of 5 malignant lymphomas in the wild type genotype (+/+), 3 under the Fe-NTA treatment and 2 under the untreated condition. (**i**) aCGH analysis of 3 malignant lymphomas in the *Mut^{yh}*^{-/-} mice (-/-), 2 under the Fe-NTA treatment and 1 under the untreated condition. Refer to the text for details.

strength of the connective tissue in mice is much lower, which may allow for the proliferation of low-grade malignant cells. These considerations are probably associated with species evolution and senescence, and thus, further studies are warranted. At the same time, we are warned by the results that murine carcinogenesis might be very different

from those of humans; however, most of the current genetically engineered animals are mice. In this sense, studies on genetically engineered rats should be promoted.

We observed, for the first time, malignant lymphoma of the kidney after Fe-NTA treatment in both the genotypes but none in the mice without Fe-NTA treatment. A repeated

Table 2 Methylation of CpG island region in selected putative tumor suppressor genes

Symbol	Locus	Full name	RCC <i>Mutyh</i> (-/-)	RCC <i>Mutyh</i> (+/+)	Malignant lymphoma (-/-) Fe-NTA treatment	Malignant lymphoma (+/+) Fe-NTA treatment	Malignant lymphoma (-/-) Untreated control	Malignant lymphoma (+/+) Untreated control
<i>Cdkn2a</i>	4 C3-C6	Cyclin-dependent kinase inhibitor 2A	0/3	0/1	1/2	1/3	0/1	1/2
<i>Trp73</i>	4 E2	Transformation related protein 73	0/3	0/1	0/2	0/3	0/1	0/2
<i>Vhl</i>	6 E3	von Hippel-Lindau tumor suppressor	0/3	0/1	0/2	0/3	0/1	0/2
<i>Mgmt</i>	7 F4	O-6-Methylguanine-DNA methyltransferase	0/3	0/1	2/2	3/3	1/1	1/2
<i>Cdh1</i>	8 D	Cadherin 1	0/3	0/1	2/2	3/3	1/1	2/2
<i>Rbp1</i>	9 E3	Retinol binding protein 1	0/3	0/1	2/2	3/3	1/1	2/2
<i>Rassf1</i>	9 F1	Ras association (RalGDS/AF-6) domain family member 1	0/3	0/1	1/2	0/3	0/1	2/2
<i>Mlh1</i>	9 F3	MutL homolog 1 (E. coli)	0/3	0/1	0/2	0/3	0/1	0/2
<i>Timp3</i>	10 C1-D1	Tissue inhibitor of metalloproteinase 3	0/3	0/1	2/2	3/3	1/1	2/2
<i>Dlk1</i>	12 E-F1	Delta-like 1 homolog (Drosophila)	2/3	1/1	2/2	3/3	1/1	2/2
<i>Dapk1</i>	13 B2	Death associated protein kinase 1	0/3	0/1	2/2	3/3	1/1	1/2
<i>Rarb</i>	14 A1-A3	Retinoic acid receptor, beta	0/3	0/1	2/2	3/3	1/1	2/2
<i>Gstp1</i>	19 A	Glutathione S-transferase pi 1	0/3	0/1	0/2	0/3	0/1	0/2

RCC, renal cell carcinoma; Fe-NTA, ferric nitrilotriacetate.

Table 3 Analysis of genomic loci for chromosomal copy number aberration (deletion or amplification) in murine and rat RCCs induced by Fe-NTA

Tumor	Number of normal loci	Number of deleted loci	Number of amplified loci	Frequency of copy number aberration (%)
Murine RCC (total 23935 sites)				
KO_1080	21250	2674	11	11.22
KO_1134	15314	8376	245	36.02
KO_1097	19242	4679	14	19.61
WT_1179	18916	3697	1322	20.97
Mean	18680.5	4856.5	398	21.95
Rat RCC (total 25503 sites)				
FB7-1	19884	5509	110	22.03
FB32-4	19836	4551	1116	22.22
FB7-7	19702	3717	2084	22.75
FB59-1	15654	9844	5	38.62
FB14-3	16244	7643	1616	36.31
BF51-1	14756	9203	1544	42.14
FB14-6	18628	5087	1788	26.96
FB21-2	18523	5961	1019	27.37
FB45-4	15917	9393	193	37.59
FB30-5	18021	6610	872	29.34
BF57-5	18216	5846	1441	28.57
Mean	17761.9	6669.5	1071.6	30.35

Fe-NTA, ferric nitrilotriacetate; RCC, renal cell carcinoma. Refer to text for details.

Fenton reaction causes chronic inflammation in the renal cortex. Thus, the occurrence of malignant B-cell type lymphoma might be similar to human inflammation-associated lymphomas, such as *Helicobacter pylori*-associated gastric lymphoma⁴⁰ or pyothorax-associated lymphoma.⁴¹ In contrast to murine RCC, lymphomas of both the genotypes revealed both amplifications and a hemiallelic loss.

Finally, we performed analyses of the methylation of the CpG islands in selected genes and found that *Dlk1* is a good candidate for a target tumor suppressor gene, which is suggested also in human RCC.⁴² Of note, the inactivation of *Dlk1* was observed not only in RCC but also in all the lymphomas examined.

In conclusion, we obtained a high incidence of murine RCC by repeated ip administration of Fe-NTA even in the cancer-resistant *C57BL/6* background²⁷ when *Mutyh*-deficient mice were used. However, the chromosomal aberrations in RCC were much less than those in rats. The results not only confirm the role of *Mutyh* in preventing Fenton reaction-induced carcinogenesis but also suggest that a murine carcinogenesis model might be more distant from human counterparts than we believed.

ACKNOWLEDGEMENTS

This work was supported by JSPS KAKENHI Grant Number JP16K15257, JP24108008 and JP17H04064 to ST, JP2221S0001 to MF and HS, JP22221004 to YN and JP15H04298 to KS, and Private University Research Branding Project to ST. This work was partly performed in the Cooperative Research Project Program of the Medical Institute of Bioregulation, Kyushu University. The BLS4 cell line was kindly provided by Dr. Tomoya Kataikai (Niigata University, Niigata, Japan). We thank Jihoon Song (Nagoya University) for technical assistance.

DISCLOSURE STATEMENT

None declared.

Abbreviations. aCGH, array-based comparative genome hybridization; Fe-NTA, ferric nitrilotriacetate; ip, intraperitoneally; PBS, phosphate-buffered saline; RCC, renal cell carcinoma.

REFERENCES

- Hussain SP, Hofseth LJ, Harris CC. Radical causes of cancer. *Nat Rev Cancer* 2003; **3**: 276–85.
- Toyokuni S. Oxidative stress as an iceberg in carcinogenesis and cancer biology. *Arch Biochem Biophys* 2016; **595**: 46–9.
- Toyokuni S. Iron-induced carcinogenesis: The role of redox regulation. *Free Radic Biol Med* 1996; **20**: 553–66.

- Toyokuni S. Role of iron in carcinogenesis: Cancer as a ferrotoxic disease. *Cancer Sci* 2009; **100**: 9–16.
- Toyokuni S, Ito F, Yamashita K, Okazaki Y, Akatsuka S. Iron and thiol redox signaling in cancer: An exquisite balance to escape ferroptosis. *Free Radic Biol Med* 2017; **108**: 610–26.
- Elmberg M, Hultcrantz R, Ekblom A *et al.* Cancer risk in patients with hereditary hemochromatosis and in their first-degree relatives. *Gastroenterology* 2003; **125**: 1733–41.
- Pearce CL, Templeman C, Rossing MA *et al.* Association between endometriosis and risk of histological subtypes of ovarian cancer: A pooled analysis of case-control studies. *Lancet Oncol* 2012; **13**: 385–94.
- Mori M, Ito F, Shi L *et al.* Ovarian endometriosis-associated stromal cells reveal persistently high affinity for iron. *Redox Biol* 2015; **6**: 578–86.
- Levrero M. Viral hepatitis and liver cancer: The case of hepatitis C. *Oncogene* 2006; **25**: 3834–47.
- Kato J, Miyanishi K, Kobune M *et al.* Long-term phlebotomy with low-iron diet therapy lowers risk of development of hepatocellular carcinoma from chronic hepatitis C. *J Gastroenterol* 2007; **42**: 330–36.
- Toyokuni S. Mechanisms of asbestos-induced carcinogenesis. *Nagoya J Med Sci* 2009; **71**: 1–10.
- Chew SH, Toyokuni S. Malignant mesothelioma as an oxidative stress-induced cancer: An update. *Free Radic Biol Med* 2015; **86**: 166–78.
- Ebina Y, Okada S, Hamazaki S, Ogino F, Li JL, Midorikawa O. Nephrotoxicity and renal cell carcinoma after use of iron- and aluminum- nitrilotriacetate complexes in rats. *J Natl Cancer Inst* 1986; **76**: 107–13.
- Li JL, Okada S, Hamazaki S, Ebina Y, Midorikawa O. Subacute nephrotoxicity and induction of renal cell carcinoma in mice treated with ferric nitrilotriacetate. *Cancer Res* 1987; **47**: 1867–9.
- Toyokuni S. The origin and future of oxidative stress pathology: From the recognition of carcinogenesis as an iron addiction with ferroptosis-resistance to non-thermal plasma therapy. *Pathol Int* 2016; **66**: 245–59.
- Akatsuka S, Yamashita Y, Ohara H *et al.* Fenton reaction induced cancer in wild type rats recapitulates genomic alterations observed in human cancer. *PLoS ONE* 2012; **7**: e43403.
- Hamazaki S, Okada S, Ebina Y, Midorikawa O. Acute renal failure and glucosuria induced by ferric nitrilotriacetate in rats. *Toxicol Appl Pharmacol* 1985; **77**: 267–74.
- Hamazaki S, Okada S, Ebina Y, Fujioka M, Midorikawa O. Nephrotoxicity of ferric nitrilotriacetate: An electron-microscopic and metabolic study. *Am J Pathol* 1986; **123**: 343–50.
- Toyokuni S, Okada S, Hamazaki S *et al.* Combined histochemical and biochemical analysis of sex hormone dependence of ferric nitrilotriacetate-induced renal lipid peroxidation in ddY mice. *Cancer Res* 1990; **50**: 5574–80.
- Toyokuni S, Mori T, Dizdaroglu M. DNA base modifications in renal chromatin of Wistar rats treated with a renal carcinogen, ferric nitrilotriacetate. *Int J Cancer* 1994; **57**: 123–8.
- Toyokuni S, Uchida K, Okamoto K, Hattori-Nakakuki Y, Hiai H, Stadtman ER. Formation of 4-hydroxy-2-nonenal-modified proteins in the renal proximal tubules of rats treated with a renal carcinogen, ferric nitrilotriacetate. *Proc Natl Acad Sci USA* 1994; **91**: 2616–20.
- Toyokuni S, Luo XP, Tanaka T, Uchida K, Hiai H, Lehotay DC. Induction of a wide range of C₂₋₁₂ aldehydes and C₇₋₁₂ acylolins in the kidney of Wistar rats after treatment with a renal carcinogen, ferric nitrilotriacetate. *Free Radic Biol Med* 1997; **22**: 1019–27.
- Kasai H. Analysis of a form of oxidative DNA damage, 8-hydroxy-2'-deoxyguanosine, as a marker of cellular oxidative stress during carcinogenesis. *Mutat Res* 1997; **387**: 147–63.

- 24 Nakabeppu Y. Regulation of intracellular localization of human MTH1, OGG1, and MYH proteins for repair of oxidative DNA damage. *Prog Nucleic Acid Res Mol Biol* 2001; **68**: 75–94.
- 25 Aretz S, Uhlhaas S, Goergens H *et al.* MUTYH-associated polyposis: 70 of 71 patients with biallelic mutations present with an attenuated or atypical phenotype. *Int J Cancer* 2006; **119**: 807–14.
- 26 Yanaru-Fujisawa R, Matsumoto T, Ushijima Y *et al.* Genomic and functional analyses of MUTYH in Japanese patients with adenomatous polyposis. *Clin Genet* 2008; **73**: 545–53.
- 27 DiGiovanni J, Bhatt TS, Walker SE. C57BL/6 mice are resistant to tumor promotion by full thickness skin wounding. *Carcinogenesis* 1993; **14**: 319–21.
- 28 Nishiyama Y, Suwa H, Okamoto K, Fukumoto M, Hiai H, Toyokuni S. Low incidence of point mutations in *H-*, *K-* and *N-ras* oncogenes and *p53* tumor suppressor gene in renal cell carcinoma and peritoneal mesothelioma of Wistar rats induced by ferric nitrilotriacetate. *Jpn J Cancer Res* 1995; **86**: 1150–58.
- 29 Tanaka T, Iwasa Y, Kondo S, Hiai H, Toyokuni S. High incidence of allelic loss on chromosome 5 and inactivation of *p15 INK4B* and *p16 INK4A* tumor suppressor genes in oxystress-induced renal cell carcinoma of rats. *Oncogene* 1999; **18**: 3793–7.
- 30 Sakamoto K, Tominaga Y, Yamauchi K *et al.* MUTYH-null mice are susceptible to spontaneous and oxidative stress induced intestinal tumorigenesis. *Cancer Res* 2007; **67**: 6599–604.
- 31 Toyokuni S, Tanaka T, Hattori Y *et al.* Quantitative immunohistochemical determination of 8-hydroxy-2'-deoxyguanosine by a monoclonal antibody N45.1: Its application to ferric nitrilotriacetate-induced renal carcinogenesis model. *Lab Invest* 1997; **76**: 365–74.
- 32 Sugimoto K, Hayakawa F, Shimada S *et al.* Discovery of a drug targeting microenvironmental support for lymphoma cells by screening using patient-derived xenograft cells. *Sci Rep* 2015; **5**: 13054.
- 33 Shimada K, Shimada S, Sugimoto K *et al.* Development and analysis of patient-derived xenograft mouse models in intravascular large B-cell lymphoma. *Leukemia* 2016; **30**: 1568–79.
- 34 Kojima Y, Hayakawa F, Morishita T *et al.* YM155 Induces apoptosis through proteasome-dependent degradation of MCL-1 in primary effusion lymphoma. *Pharmacol Res* 2017; **120**: 242–51.
- 35 Aoki T, Shimada K, Sakamoto A *et al.* Emetine elicits apoptosis of intractable B-cell lymphoma cells with *MYC* rearrangement through inhibition of glycolytic metabolism. *Oncotarget* 2017; **8**: 13085.
- 36 Ito F, Nishiyama T, Shi L *et al.* Contrasting intra- and extracellular distribution of catalytic ferrous iron in ovalbumin-induced peritonitis. *Biochem Biophys Res Commun* 2016; **476**: 600–606.
- 37 Yamamoto E, Suzuki H, Yamano H-O *et al.* Molecular dissection of premalignant colorectal lesions reveals early onset of the CpG island methylator phenotype. *Am J Pathol* 2012; **181**: 1847–61.
- 38 Edwards JH. The Oxford Grid. *Ann Hum Genet* 1991; **55**: 17–31.
- 39 Jiang L, Akatsuka S, Nagai H *et al.* Iron overload signature in chrysotile-induced malignant mesothelioma. *J Pathol* 2012; **228**: 366–77.
- 40 Parsonnet J, Hansen S, Rodriguez L *et al.* Helicobacter pylori infection and gastric lymphoma. *New Engl J Med* 1994; **330**: 1267–71.
- 41 Nakatsuka S-I, Yao M, Hoshida Y, Yamamoto S, Iuchi K, Aozasa K. Pyothorax-associated lymphoma: A review of 106 cases. *J Clin Oncol* 2002; **20**: 4255–60.
- 42 Kawakami T, Chano T, Minami K, Okabe H, Okada Y, Okamoto K. Imprinted DLK1 is a putative tumor suppressor gene and inactivated by epimutation at the region upstream of GTL2 in human renal cell carcinoma. *Hum Mol Genet* 2006; **15**: 821–30.

SUPPORTING INFORMATION

Additional Supporting Information may be found in the online version of this article at the publisher's website.

Figure S1 Histograms of the moving averages of the signal log₂ ratios for all the array-CGH data used for the inter-species comparison.

Figure S2 Bar charts of the frequencies of the genomic sites with a normal or aberrated copy number in each array-CGH profile of murine and rat RCC.

Figure S3 Plot of signal log₂ ratio along chromosome 4 for one representative aCGH result from an RCC sample in a *Mutyh*^{-/-} mouse (NO. 1080).

Table S1 Primer sequences for pyrosequencing methylayion analysis

Table S2 Sequences of PCR primers used to amplify genomic regions including exonic portions of *Cdkn2*

Table S3 Macroscopic details of each tumor